Electromagnetic tunneling through conjugated single-negative metamaterial pairs and double-positive layer with high-magnetic fields

Yuanyuan Chen (陈园园)*, Shanhong Huang (黄闪红), Xiaona Yan (阎晓娜), and Jielong Shi (施解龙)

Department of Physics, Shanghai University, Shanghai 200444, China

**Corresponding author: cyyuan@staff.shu.edu.cn*

Received April 10, 2014; accepted June 18, 2014; posted online September 28, 2014

We show that resonant tunneling of electromagnetic (EM) fields can occur through a six-layer structure consisting of two pairs of bilayer slabs: one being an epsilon-negative layer and the other being a mu-negative layer with a double-positive (DPS) medium and air. This type of tunneling is accompanied by high-magnetic field. The Poynting vector distributions and the material dissipation are studied. Our results demonstrate that the EM field in the structure is controlled flexibly by single-negative media and DPS slab. Therefore, this structure has potential applications in wireless energy transfer.

OCIS codes: 160.3918, 240.7040.

doi: 10.3788/COL201412.101601.

In the past three decades, there has been a considerable interest in the tunneling of electromagnetic (EM) wave for its practical applications in many various aspects. With the advancement in the field of metamaterials, many unusual physical properties have been exhibited[1–5] and the tunneling in metamaterials has attracted significant attention[6,7]. The metamaterials include double-negative and single-negative (SNG) materials[8,9]. SNG material with negative relative permittivity (ε-negative (ENG)) or negative relative permeability (μ-negative (MNG)) should be opaque media because the EM wave is evanescent. Under proper conditions, the tunneling through certain structures consisting of one or more SNG materials can be achieved[10–15].

Recently, non-radiative EM transfer, enabling efficient and safe wireless energy transfer has received substantial interest[16–21]. This proposed scheme is based on magnetic resonances (the fact that two same frequency resonant objects tend to couple, while interacting weakly with other off-resonant environmental objects) and resonant evanescent coupling through the overlap of the non-radiative near fields of the two objects. Magnetic resonances are particularly suitable for everyday applications because most of the common materials do not interact with magnetic fields, so interactions with environmental objects are suppressed even further. There is a strong EM coupling between resonant objects, but the coil-based systems are bulky in order to reach high efficiencies.

Recently, research on radiative and non-radiative energy transfer in metamaterial has been reported[22,23]. The possible application of wireless energy transfer with a sandwich structure consisting of MNG medium, air, and ENG medium was investigated[23]. The distribution of electric and magnetic fields in some tunneling structure consisting of SNG media or double-positive (DPS) media can be controlled[24–27]. Inspired by the tunneling of EM wave and field modification in SNG materials, we investigate a different scheme of non-radiative energy transfer in a multi-layer structure similar to Feng *et al.*[23]. The difference is that we have placed two pairs of ENG/MNG couple layers on the two ends and there is one more DPS layer on the incident side of air. The results show our structure is superior and controllable because of the following reasons: 1) the magnetic field is enhanced and the stronger magnetic field is located on the receiving terminal; 2) the DPS material accelerates the decay of the electric field, so the electric field in the air is small; 3) the energy of tunneling ends if the receiving terminal is removed.

The geometry is illustrated in the Cartesian coordinate system ($\bar{x}$, $\bar{y}$, and $\bar{z}$) of Fig. 1. Without loss of generality, we consider a multi-layer structure in air. A, B, C, and D represent ENG medium, MNG medium, DPS medium, and air, respectively. ε and μ are relative permittivity and relative permeability of media. Here each slab (including DPS) is isotropic, linear, and homogeneous. We assume the problem to be

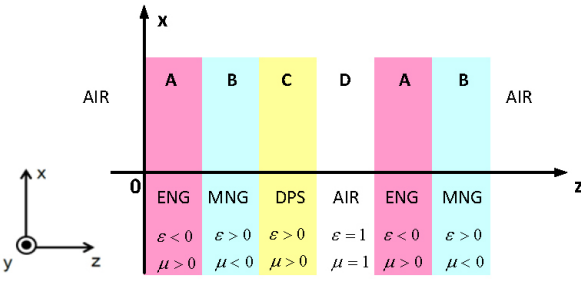

Fig. 1. Heterostructure containing SNG materials in air.

two-dimensional (2D), that is, all quantities are independent of the y-coordinate. We investigate the tunneling phenomenon in this structure.

Consider that a transverse electric wave having the electric-field vector $\bar{E}$ parallel to $\bar{y}$ is normally incident onto this composite structure along the z-axis. The field components E and H are continuous across the interfaces and a unimodular field-transfer matrix M_j relates the field amplitudes E_j and H_j at Z_j to the corresponding amplitudes at z_{j-1}:

$$\begin{bmatrix} E_{j-1} \\ H_{j-1} \end{bmatrix} = \mathbf{M}_j \begin{bmatrix} E_j \\ H_j \end{bmatrix}, \tag{1}$$

where $\mathbf{M}_j$ is given by[28]

$$\mathbf{M}_j = \begin{bmatrix} \cos\delta_j & \frac{\mathrm{i}}{\sigma_j}\sin\delta_j \\ \mathrm{i}\sigma_j \sin\delta_j & \cos\delta_j \end{bmatrix}, \tag{2}$$

with $\sigma_j = \varepsilon_j / n_j$ and $\delta_j = k_j d_j$, where ε_j, n_j, k_j, and d_j denote the permittivity, the refractive index, the wave number, and the thickness of each layer, respectively. For SNG media, $n_j = -\mathrm{i}\sqrt{|\varepsilon_j \mu_j|}$, $k_j = -\mathrm{i}k_0\sqrt{|\varepsilon_j \mu_j|}$, and $k_0 = \omega/\mathrm{c}$. The transfer matrix of the structure consisting of six layers is given by the product of the respective transfer matrices for the individual layers:

$$\mathbf{M} = \prod_{j=1}^{6} \mathbf{M}_j. \tag{3}$$

The reflection coefficient is derived by the transfer matrix:

$$r = \frac{\mathbf{M}_{11} + \mathbf{M}_{12} - \mathbf{M}_{21} - \mathbf{M}_{22}}{\mathbf{M}_{11} + \mathbf{M}_{12} + \mathbf{M}_{21} + \mathbf{M}_{22}}, \tag{4}$$

where M_{ij} (i, j = 1, 2) are the elements of the matrix $\mathbf{M}$. We can derive the condition for the total transmission by zeroing the reflection coefficient, which also corresponds to the occurrence of the tunneling. For the six-layer structure, the expression of reflection coefficient is very complex. For simplification, we refer to the "matched pair" condition given by Alù *et al.*[10] for the purpose of preliminary design. Assume the ENG/MNG bilayer are paired, that is, $\delta_A = \delta_B$, ENG is non-magnetic ($\mu_A = 1$), MNG is non-electric ($\varepsilon_B = 1$), and the permittivity and permeability of DPS are equal, which means $\sigma_C = \sigma_D = 1$. By substituting Eqs. (2) and (3) into Eq. (4) and zeroing the reflection coefficient, the condition for zero reflection is derived as

$$\tan(\delta_C + \delta_D) = \frac{1/2(1+\sigma_B^4)(\cos 2\delta_B - 1) + \sigma_B^2(\cos 2\delta_B - 1)}{(\sigma_B^3 + \sigma_B)\sin 2\delta_B}. \tag{5}$$

When Eq. (5) is satisfied, the interface modes at different interfaces of MNG and ENG layers can resonantly couple to each other, leading to the emergence of the tunneling mode.

Now, we use a Drude model to describe SNG materials: ENG: $\varepsilon_A = 1 - \frac{\omega_{\mathrm{ep}}^2}{\omega^2}$, $\mu_A = 1$, ω_{ep} is the plasma frequency; MNG: $\varepsilon_B = 1$, $\mu_B = 1 - \frac{\omega_{\mathrm{mp}}^2}{\omega^2}$, ω_{mp} is the magnetic resonance frequency; where $\omega = 2\pi f$ and the unit of f is GHz.

In the following calculations, we set DPS layer as air, that is, $\varepsilon_c = \mu_c = 1$, and choose a set of parameters of $\omega_{\mathrm{ep}} = \omega_{\mathrm{mp}} = 8.2$ GHz, $d_A = d_B = d_C = d_D = 20$ mm. The transmittance can be obtained by Eq. (4), $T = 1 - r^*$. Figure 2(a) shows the corresponding transmittance response as a function of frequency, and it is clear that the energy totally tunnels through the composite structure at $f_0 = 0.353$ GHz. The EM-field distribution of the tunneling mode with its frequency at 0.353 GHz is shown in Fig. 2(b). The electric field is the maximum at the MNG–air interface and the magnetic field has the same maximum value at the air–ENG interface. This result is similar to that in Ref. [23].

Next, we change the parameters of DPS layer: $\varepsilon_c = 5$, $\mu_c = 5$. Figure 3 shows that the transmittance peak shifts to the low frequency slightly and the spectral width of the tunneling mode narrows a little. The electric field and magnetic field are still localized at the MNG–air interface and the air–ENG interface with the same maximum, but the field amplifications are higher than that when DPS is air. The magnetic field reaches higher magnitude after being twice amplified, and the slope of electric field in DPS layer is sharper than that in the air.

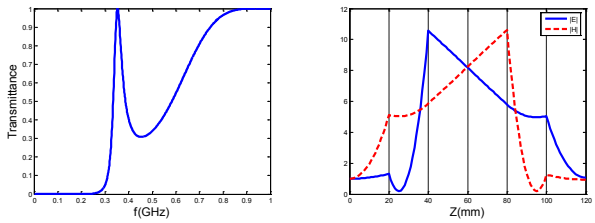

(a) (b)

Fig. 2 (a) Corresponding transmittance response to frequency when DPS layer is air and (b) the EM-field distribution of the tunneling mode at 0.353 GHz (normalized by the incident fields).

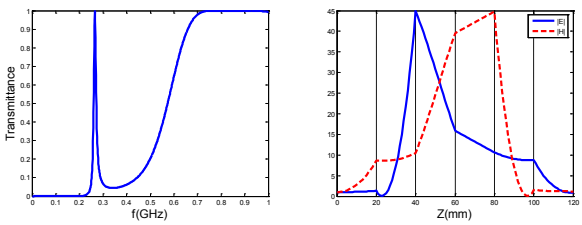

(a) (b)

Fig. 3 (a) Transmittance frequency response for DPS: $\varepsilon_c = 5$, $\mu_c = 5$ and (b) the EM-field distribution of the tunneling mode at 0.265 GHz (normalized by the incident fields).

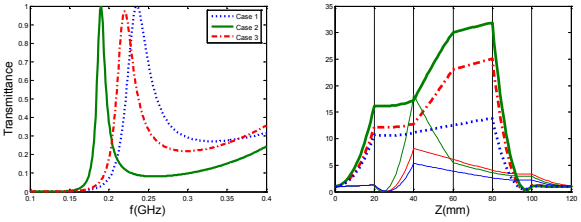

(a) (b)

Fig 4 (a) Transmittance frequency response for three cases and (b) electric field (thin lines) and the magnetic-field (thick lines) distributions of the tunneling modes at 0.235 GHz (Case (1): dotted line); 0.19 GHz (Case (2): solid line); 0.22 GHz (Case (3): dash-dotted line).

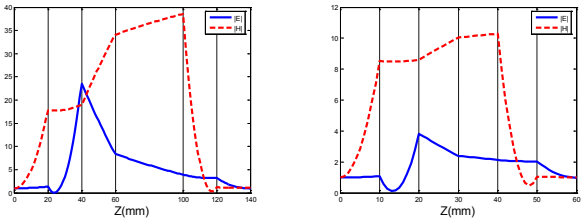

(a) (b)

Fig 5 (a) EM-field distribution corresponding to the tunneling modes: (a) $f = 0.181$ GHz, $d_A = d_B = d_C = 20$ mm, and $d_D = 40$ mm and (b) $f = 0.131$ GHz, $d_A = d_B = d_C = d_D = 10$ mm. Other parameters follow Case (2) in Fig. 4.

The electric field and magnetic field are localized at the different interfaces as shown in Fig. 3(b). Therefore, the structure at the left side of air layer can be considered as a transmitting device, whereas the right side of air layer can be considered as a receiving device. In the following, we hope to obtain stronger magnetic field to increase the coupling efficiency and keep weaker electric field in the air for safety.

By Maxwell's equations, it is derived that $\frac{\partial E_y}{\partial z} = -\mathrm{i}\omega\mu_0\mu H_x$ and $\frac{\partial H_x}{\partial z} = \mathrm{i}\omega\varepsilon_0\varepsilon E_y$, where ε_0 and μ_0 are the vacuum permittivity and permeability, and ε and μ are the relative permittivity and permeability. It means that the electric field changing with distance is related to the permeability of structure, whereas the magnetic field changing with distance is related to the permittivity of structure. So we can restrain the enhancement of the electric field by reducing the value of permeability of the MNG media. In the following, we set $\omega_{\mathrm{ep}} = 8.2$ GHz and $\omega_{\mathrm{mp}} = 5.03$ GHz and consider three cases: 1) DPS: air for dotted line; 2) DPS: $\varepsilon_c = 5$ and $\mu_c = 5$ for solid line; 3) DPS: $\varepsilon_c = 5$ and $\mu_c = 1$ for dash-dotted line. The results in Fig. 4 show that the electric field and magnetic field are no longer enhanced as same scale. From Table 1, it is clear that the absolute value of the permeability of MNG $|\mu_B|$ is less than that of the permittivity of ENG $|\varepsilon_A|$, so the enlargement of electric field is restrained. In Case (2), the DPS can increase the magnetic field further, although the electric field is also increased at the MNG–air interface, it is reduced quickly in the DPS layer. In Case (3), where the DPS is a dielectric medium with $\varepsilon_c = 5$ and $\mu_c = 1$, and the condition for zero reflection Eq. (5) is not followed, the transmission is less than 1, but the EM-field distribution is still similar to Case (2). Case (2) is superior to Case (3) due to the lower electric field in the air and the higher magnetic field at the air–MNG interface.

Figure 5 shows the EM-fields of the tunneling modes for different thicknesses of layers. The transmittance peak has a red-shift with the increase in air layer, and the bandwidth of the tunneling mode narrows. But this does not affect the energy transfer, so we can achieve energy transfer at a relatively long distance. And the decrease in thickness for layers will suppress the enhancement of magnetic field and therefore we need to balance between high-efficient coupling and structure size.

Next we address the question of what will happen if the pair of ENG/MNG media at the right side of air layer are removed or are changed as common dielectric medium. Figure 6 shows the transmittance and the reflectance of the structure for different conditions. When the receiving terminal at the right side of air layer is removed or changed, the transmittance drops rapidly, whereas the reflectance increases, and the larger the parameter of the dielectric medium is, the lower is the transmittance. Therefore, the tunneling phenomenon will no longer exists without the proper terminal, which means a flexible switch to energy transfer and exemption from energy loss.

Table 1. Permittivity and Permeability Parameters of ENG and MNG corresponding to the different Frequencies of Tunneling Modes for three Cases

Frequency of Tunneling Mode f(GHz)		**ENG** (ε_{A}, μ_{A})	**MNG** (ε_{B}, μ_{B})	**DPS** (ε_{C}, μ_{C})
Case (1)	0.235	(−29.84, 1)	(1, −10.60)	(1, 1)
Case (2)	0.19	(−46.18, 1)	(1, −16.75)	(5, 5)
Case (3)	0.22	(−34.19, 1)	(1, −12.24)	(5, 1)

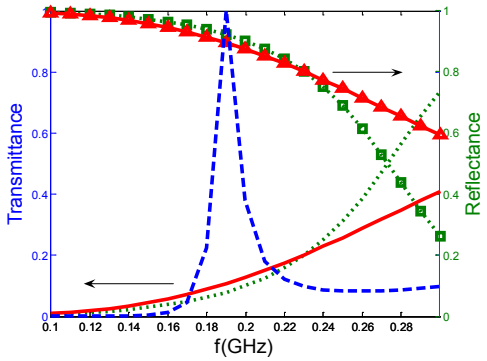

Fig. 6. Transmittance (without marker) and the reflectance (with marker) frequency response for the different terminals behind air: ENG/MNG (dashed line), air (solid line), common dielectric material (dotted line), and the parameters are $\varepsilon = 9$, $\mu = 1$.

Moreover, to investigate the energy transfer, the energy flux in the composite structure is also studied. The energy flux density is defined by the Poynting vector, that is,

$$\vec{S} = \vec{E} \times \vec{H}. \tag{6}$$

The real and imaginary parts of the Poynting vector for a tunneling mode through multi-slabs are shown in Fig. 7. The real part of the Poynting vector is uniform and equal unity in the structure, implying the complete tunneling of the incident wave, whereas the imaginary part of the Poynting vector has its peaks at ENG–MNG interfaces in Fig. 7(a) and at ENG–MNG and MNG–DPS interfaces in Fig. 7(b). This exhibits the presence of resonant energy in these layers, which, as was explained by by Alù *et al.*[10], and can be regarded as a resonance phenomenon.

We start from the same configuration above, but now assuming a more realistic lossy Drude model for the ENG and MNG media:

$$\text{ENG: } \varepsilon_A = 1 - \frac{\omega_{\text{ep}}^2}{\omega(\omega + \mathrm{i}\gamma_1)}, \mu_A = 1,$$

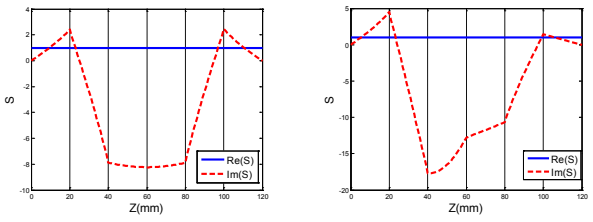

(a) (b)

Fig. 7 (a) Distribution of the real and imaginary parts of the normalized Poynting vector in the structure: (a) the tunneling mode at 0.353 GHz in Fig. 2(b), DPS: air and (b) the tunneling mode at 0.19 GHz for Case (2) in Fig. 4(b), DPS: $\varepsilon_c = 5$, $\mu_c = 5$. The normalization is with respect to the value of the Poynting vector of the incident wave.

$$\text{MNG: } \varepsilon_B = 1, \mu_B = 1 - \frac{\omega_{\text{ep}}^2}{\omega(\omega + \mathrm{i}\gamma_2)},$$

where $\gamma_1 = \gamma^* \omega_{\text{ep}}$ and $\gamma_2 = \gamma^* \omega_{\text{mp}}$ are the damping coefficients. γ is often indicated as the order of 10^{-3} in many experimental and simulation studies[29–33] and the uncommon larger damping factor was given as $\gamma = 0.01$ by Reza *et al.*[34].

Figure 8 shows the transmittance, EM field, and the energy flux in the structure for different loss levels. The loss does not significantly affect the position of the peak frequency, but the transmittance reduces rapidly with the higher material loss as shown in Fig. 8(a). The real part of the Poynting vector decays from unity with the distance, and thus more loss, more decay. The energy flux density at the terminal is less than half of the initial energy when $\gamma = 0.02$, but there is still "resonance" phenomenon in the structure, and the electric and magnetic fields are localized at different interfaces in Figs. 8(b) and (c). The tunneling will stop functioning for high-loss levels. When the realistic loss level γ is less than 0.01, high transmittance can be carried through the structure. However, when γ is more than 0.02, the transmission efficiency is low. For practical

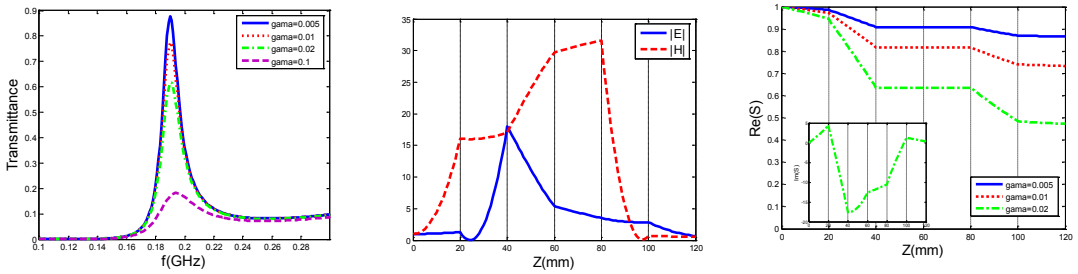

(a) (b) (c)

Fig. 8 (a) Transmittance frequency response for different loss factors, (b) EM-field distribution of the tunneling mode of 0.19 GHz for $\gamma = 0.02$, and (c) the normalized Poynting vector in the structure, and inset is the imaginary part of Poynting vector for $\gamma = 0.02$.

metamaterial, the loss of less than 0.01 is not difficult to be achieved. Therefore, our approach could be applicable to wireless power transfer with metamaterial.

In conclusion, we illustrate an EM-field resonant tunneling mechanism that takes place by pairs of ENG/MNG slab with a DPS layer and air layer. And we analyze field distribution and the Poynting vector in the structure. The asymmetrical electric field and magnetic field of the tunneling mode are separated and localized at different interfaces of two sides of air, respectively. The enhancement of the magnetic field and the suppression of electrical field are controlled by the DPS. The ENG and MNG material loss is also taken into account. Compared with previous work, the electric field and the magnetic field in our structure are amplified with different ratios, and the higher amplified magnetic field is localized at the interface of ENG–air. Although the electric field is enhanced at first, it decays rapidly in the DPS layer. Therefore, this composite structure of SNG couples and DPS provides an improved path to the design of wireless transmission devices which are more efficient and have greater potential for tunability.

This work was supported by the National Natural Science Foundation of China under Grant No. 11274225.

References

1. D. R. Smith, W. J. Padilla, D. C. Vier, S. C. Nemat-Nasser, and S. Schultz, Phys. Rev. Lett. **84,** 4184 (2000).
2. J. B. Pendry, Phys. Rev. Lett. **85,** 3966 (2000).
3. A. Grbic and G. V. Eleftheriades, Phys. Rev. Lett. **92,** 117403 (2004).
4. D. Schurig, J. J. Mock, B. J. Justice, S. A. Cummer, and J. B. Pendry, Science **314,** 977 (2006).
5. Y. Chen, Y. Fang, S. Huang, and J. Shi, Chin. Opt. Lett. **11,** 061602 (2013).
6. J. D. Baena, L. Jelinek, R. Marqués, and F. Medina, Phys. Rev. B **72,** 075116 (2005).
7. M. Silveirinha and N. Engheta, Phys. Rev. Lett. **97,** 157403 (2006).
8. D. Cheng and L. Deng, Chin. Opt. Lett. **11,** 224 (2013).
9. M. Z. Ali, Chin. Opt. Lett. **11,** 040501 (2013).
10. A. Alù and N. Engheta, IEEE Trans. Antennas Propag. **51,** 2558 (2003).
11. H. Jiang, H. Chen, H. Li, Y. Zhang, J. Zi, and S. Zhu, Phys. Rev. E **69,** 066607 (2004).
12. L. Dong, G. Du, H. Jiang, H. Chen, and Y. Shi, J. Opt. Soc. Am. B **26,** 1091 (2009).
13. W. Lin, C. Wu, and S. Chang, Prog. Electromagnet. Res. **107,** 253 (2010).
14. Y. Ding, Y. Li, H. Jiang, and H. Chen, PIERS Online **6,** 109 (2010).
15. E. Cojocaru, Prog. Electromagnet. Res. **113,** 227 (2011).
16. A. Kurs, A. Karalis, R. Moffatt, J. D. Joannopoulos, P. Fisher, and M. Soljacic, Science **317,** 83 (2007).
17. M. Soljacic, E. H. Rafif, and A. Karalis, Phys. Rev. **75,** 1 (2007).
18. A. Karalis, J. D. Joannopoulos, and M. Soljacic, Ann. Phys. **323,** 34 (2008).
19. R. E. Hamam, A. Karalis, J. D. Joannopoulos, and M. Soljacic, Ann. Phys. **324,** 1783 (2009).
20. A. Kurs, R. Moffatt, and M. Soljacic, Appl. Phys. Lett. **96,** 044102 (2010).
21. J. Park, Y. Tak, Y. Kim, Y. Kim, and S. Nam, IEEE Trans. Antennas Propag. **59,** 1769 (2011).
22. K. Joulain, J. Drevillon, and P. Ben-Abdallah, Phys. Rev. B **81,** 165119 (2010).
23. T. Feng, Y. Li, H. Jiang, Y. Sun, L. He, H. Li, Y. Zhang, Y. Shi, and H. Chen, Phys. Rev. E **79,** 026601 (2009).
24. L. Zhou, W. Wen, C. T. Chan, and P. Sheng, Phys. Rev. Lett. **94,** 243905 (2005).
25. Y. Q. Ding, Y. H. Li, H. T. Jiang, and H. Chen, Opt. Commun. **284,** 1589 (2011).
26. G. Castaldi, I. Gallina, V. Galdi, A. Alu, and N. Engheta, Phys. Rev. B **83,** 081105 (2011).
27. G. Castaldi, V. Galdi, A. Alù, and N. Engheta, J. Opt. Soc. Am. B **28,** 2362 (2011).
28. P. Yeh, *Optical Waves in Layered Media* (Wiley, 1988).
29. S. Zhang, W. Fan, N. C. Panoiu, K. J. Malloy, R. M. Osgood, and S. R. J. Brueck, Phys. Rev. Lett. **95,** 137404 (2005).
30. G. Dolling, M. Wegener, C. M. Soukoulis, and S. Linden, Opt. Lett. **32,** 53 (2007).
31. N. Liu, M. Mesch, T. Weiss, M. Hentschel, and H. Giessen, Nano Lett. **10,** 2342 (2010).
32. J. Zhou, T. Koschny, and C. M. Soukoulis, Opt. Express **16,** 11147 (2008).
33. G. Dolling, C. Enkrich, M. Wegener, C. M. Soukoulis, and S. Linden, Opt. Lett. **31,** 1800 (2006).
34. A. Reza, M. M. Dignam, and S. Hughes, Nature **455,** E10 (2008).